machines

MDPI

Article

Dynamic Evaluation Method of Straightness Considering Time-Dependent Springback in Bending-Straightening Based on GA-BP Neural Network

Qingshun Kong [1,2,*] and Zhonghua Yu [1,2]

[1] School of Mechanical Engineering, Zhejiang University, Hangzhou 310027, China; 12025007@zju.edu.cn
[2] State Key Laboratory of Fluid Power and Mechatronic Systems, Zhejiang University, Hangzhou 310027, China
* Correspondence: kongqingshun@zju.edu.cn

Abstract: There is a time-dependent springback phenomenon seen during the process of the bending-straightening of slender shafts, which has a great influence on the evaluation of straightness after straightening, creating a risk of misjudgment. This paper presents a dynamic evaluation method of straightness considering time-dependent springback in the bending-straightening process. Firstly, based on viscoelastic mechanics and bending-straightening, the influencing factors of time-dependent springback were analyzed on the basis of certain assumptions, including straightening stroke δ_C, fulcrum distance L, instantaneous springback δ_b, straightening time t_s, and straightening force F_{max}. As the main part of the proposed dynamic evaluation method, the GA-BP neural network is used to establish a model for fast prediction of time-dependent springback in straightening, and it is compared with the linear regression model. The maximum prediction error of the GA-BP model was 0.0038 mm, which was much lower than that of the regression model, at 0.014 mm. The root mean square error (RMSE) of the GA-BP model was 0.0042, and that of the regression model was 0.0098. Finally, the effectiveness of the dynamic straightness evaluation method considering time-dependent springback is verified by experiments. Finally, the sensitivity and relative importance of the influencing factors are analyzed, and the order is $\delta_C > t_s > F_{max} > L > \delta_b$.

Keywords: bending-straightening; time-dependent springback; straightness; GA-BP neural network

check for updates

Citation: Kong, Q.; Yu, Z. Dynamic Evaluation Method of Straightness Considering Time-Dependent Springback in Bending-Straightening Based on GA-BP Neural Network. *Machines* **2022**, *10*, 345. https://doi.org/10.3390/machines10050345

Academic Editors: Zhenzhong Wang, Ri Pan and Xu Yang

Received: 13 April 2022
Accepted: 5 May 2022
Published: 7 May 2022

Publisher's Note: MDPI stays neutral with regard to jurisdictional claims in published maps and institutional affiliations.

Copyright: © 2022 by the authors. Licensee MDPI, Basel, Switzerland. This article is an open access article distributed under the terms and conditions of the Creative Commons Attribution (CC BY) license (https://creativecommons.org/licenses/by/4.0/).

1. Introduction

As an important part of support and transmission, a bar workpiece is widely used in mechanical products. The straightness of the bar workpiece not only affects the accuracy of assembly but also affects the performance of the equipment. Thus, improving the straightness of the bar workpiece has been widely studied [1]. At present, straightening is an effective method to improve the straightness of rod parts. Straightening methods are divided into the following categories: roller straightening, stretching straightening, and bending-straightening, among others. Bending-straightening is widely used due to its high precision and suitability for various sections of the workpiece [2].

The basic principle of bending-straightening is to make reverse the bending of the workpiece and produce elastic-plastic deformation. After the force is removed, the workpiece bounces back, finally having the straightness of the workpiece meet certain requirements [3]. When straightening begins, the shaft is placed on two support blocks, usually at the midpoint of the two blocks where the deflection of the shaft is greatest, and the position of the straightening load is also at this midpoint [4,5]. When the initial deflection δ_0 at the midpoint is measured, the straightening system calculates the straightening stroke δ_C. When straightening is complete, the instantaneous springback of the midpoint of the shaft is δ_b. If Equation (1) is satisfied, the straightness of the shaft meets the requirements.

$$|\delta_C - \delta_b - \delta_0| \leq Straightness\ requirement \quad (1)$$

Research on bending-straightening has been developing for many years. Li et al. [6] established a load-deflection bending-straightening model, studied the relationship between the load and deflection, and finally verified the validity of the model through finite element simulation and experiments. Zhao et al. [7] developed a one-time leveling control strategy for multi-point bending and proposed a method to obtain the corresponding straightening parameters by discretization and linearization of theoretical torque curves. They also introduced load-correction coefficients. Finally, the validity of the proposed method was verified by finite element analysis and experiments. Mao et al. [8] proposed a bending-straightening algorithm for seamless welded rail. The bending-straightening model was established by simplifying the section. In order to reduce the error caused by section simplification, the shape compensation coefficient was introduced, and the effectiveness of the proposed algorithm was verified through experiments.

Although there have been many studies on bending–straightening, in the process of developing a straightening machine, we found that, for slender shafts, there is a time-dependent springback phenomenon seen in the straightening process. Specifically, when the straightening actuator is separated from the shaft, the shaft will continue to spring back slowly; this has not been reported in the field of straightening. In Figure 1, δ_t is the time-dependent springback.

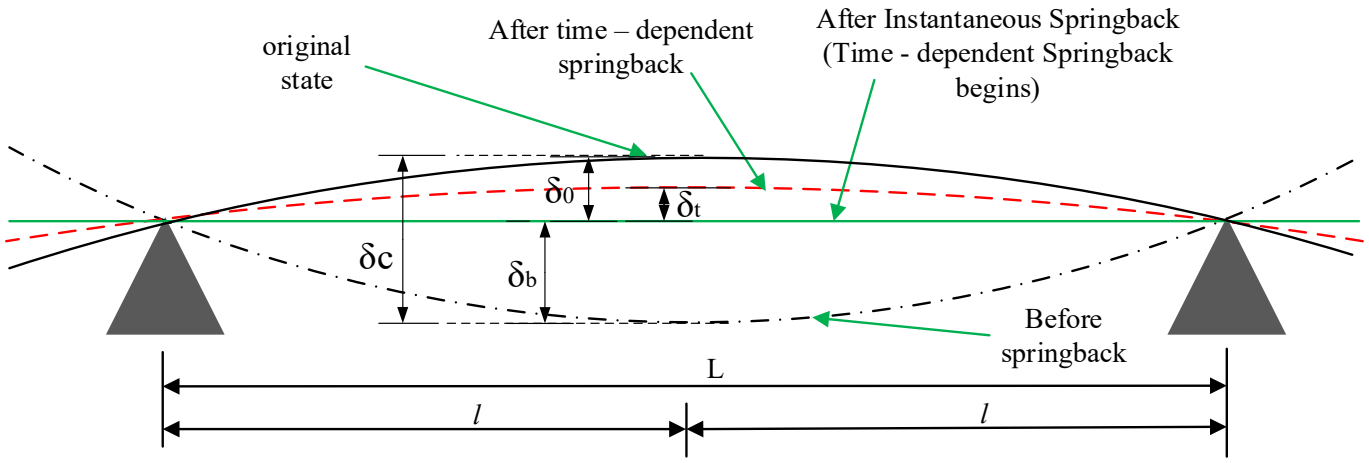


Figure 1. Bending-straightening principle.

To date, some scholars have carried out research on time-dependent springback in other fields. Lim H et al. [9] conducted draw–bend tests on different types of high-strength steel, and the time-dependent springback angle reached saturation after about one day. Sun and E. [10] conducted a uniaxial tensile test on AC170PX aluminum alloy and studied the time-dependent springback of the sample under different tensile and strain rates. They found that the time-dependent springback was related to both rates.

The finite element method (FEM) is an effective tool, often used for various types of research, and the development of this approach is becoming increasingly refined. For example, Pinnola F P et al. [11] studied the bending behavior of straight elastic beam systems with different scales by using the stress-driven, non-local, continuum mechanics method, and developed an effective calculation method based on a non-local, two-node, finite element method. At present, the finite element method is mainly used in the prediction of time-dependent springback. Liu and E [12] used this method to predict the time-dependent springback of 1Cr18Ni9Ti stainless steel tubes. They adopted the one-dimensional idealization of the two-layer viscoelastic model [13], fitted the parameters of the model by uniaxial tensile testing, and then used finite element software to predict the time-dependent springback. The predicted results are close to the experimental values. Fu and E [14] adopted creep theory and then used finite element software for prediction. The prediction result was small, and the adjustment coefficient was introduced to make

the prediction result close to the experimental value. Li et al. [15] used creep theory and a viscoelastic model to predict the time-dependent springback of high-strength titanium tubular materials.

However, straightening is different from other processing methods, and the processing parameters are not the same. Secondly, although the finite element method generates results close to experimental values, they still have a large error due to the idealization of material parameters. Moreover, the finite element method is time-consuming and cannot be directly used in engineering applications.

There are few studies on the mathematical model of time-dependent springback. Using the theory of viscoelasticity, Sun [16] predicted the time-dependent springback of DP600 under uniaxial tension. The predicted result was close to the experimental value and could well reflect the springback law. However, elastic-plastic deformation is involved in the straightening process, the mechanism of time-dependent springback is very complicated, and it is difficult to establish a mathematical model.

Although less attention is paid to time-dependent springback in the field of straightening, we found that the time-dependent springback had a great impact on the straightness evaluation of the slender shaft after straightening when we developed the straightening equipment. Considering the efficiency of straightening, a key procedure after straightening—the evaluation of the straightness of the shaft—will be carried out immediately after straightening. We connect the ends of the shaft as a reference. As shown in Figure 2, we define the deflection value of the shaft as negative when the position of maximum deflection is lower than the reference, and positive when it is higher than the reference. Range ① is the evaluation standard without considering time-dependent springback. When the maximum deflection of the shaft is in range ①, the straightness error of the shaft can be judged to meet the requirements. However, after straightening, there will be time-dependent springback in the shaft, which makes the evaluation of straightness after straightening risky. After straightening, for example, when the straightness error of the shaft is in range ②, it is qualified without considering time-dependent springback, but time-dependent springback ultimately causes the straightness error of the shaft to exceed range ①. Thus, the straightness error does not meet the straightness requirements, and there will be β risk. If the straightness error of the shaft is in the range ③, it means the shaft is unqualified without considering time-dependent springback. However, due to the existence of time-dependent springback, the maximum deflection of the shaft is eventually within range ①, and the straightness error of the shaft finally meets the requirements. So, there is α risk. Therefore, the motivation of this paper is to propose a dynamic evaluation method of straightness considering time-dependent springback so as to reduce the two types of risk.

Therefore, understanding how to reduce the risk of straightness evaluation is critical. The key problem in this regard is determining the dynamic acceptability limit of straightness, and the key problem in determining this acceptability limit is predicting the time-dependent springback.

According to the literature review, there is no good method to predict the time-dependent springback at present, and it cannot be directly applied in engineering projects. However, machine learning [17–19] methods are a better choice for predicting time-dependent springback. In particular, the BP neural network is widely used in this regard. Liu et al. [20] used a BP neural network to predict the farthest distance and maximum velocity of flame propagation and achieved good prediction results. Wang et al. [21] established a short-term solar irradiance prediction model based on the BP neural network and time series and verified its validity through simulation results. Liu et al. [22] established a dynamic prediction model for the operating parameters of a nuclear power plant using a back-propagation neural network, and the verification results show that the model has high accuracy. However, the BP neural network has disadvantages such as slow learning speed and ease of falling into local minimum [23,24]. The genetic algorithm (GA) [25,26] has the ability of global searching and can make up for the shortcomings of the BP neural network.

The GA-BP algorithm is also widely used in prediction and has achieved good prediction results. Yao et al. [27] used a BP neural network optimized by the genetic algorithm to predict the foreclosure property market trend during the pandemic, providing an effective method for predicting housing prices. Wang et al. [28] used a wind-speed prediction model based on improved empirical mode decomposition and the GA-BP neural network method and verified the accuracy of the model with MATLAB. The results were relatively accurate. He et al. [29] established a prediction model for mold breakout prediction in slab continuous casting based on the GA-BP neural network and logic rules, and the prediction accuracy reached 100%. According to our literature survey, there is no relevant research that applies the GA-BP algorithm to the prediction of time-dependent springback in the straightening process. In this paper, the GA-BP algorithm is used to predict the time-dependent springback, offering a new idea for the research of time-dependent springback in straightening. However, as the model input is a key factor affecting the accuracy of the algorithm, no one has explored the influencing factors in the straightening process, which is also an important contribution of our paper.

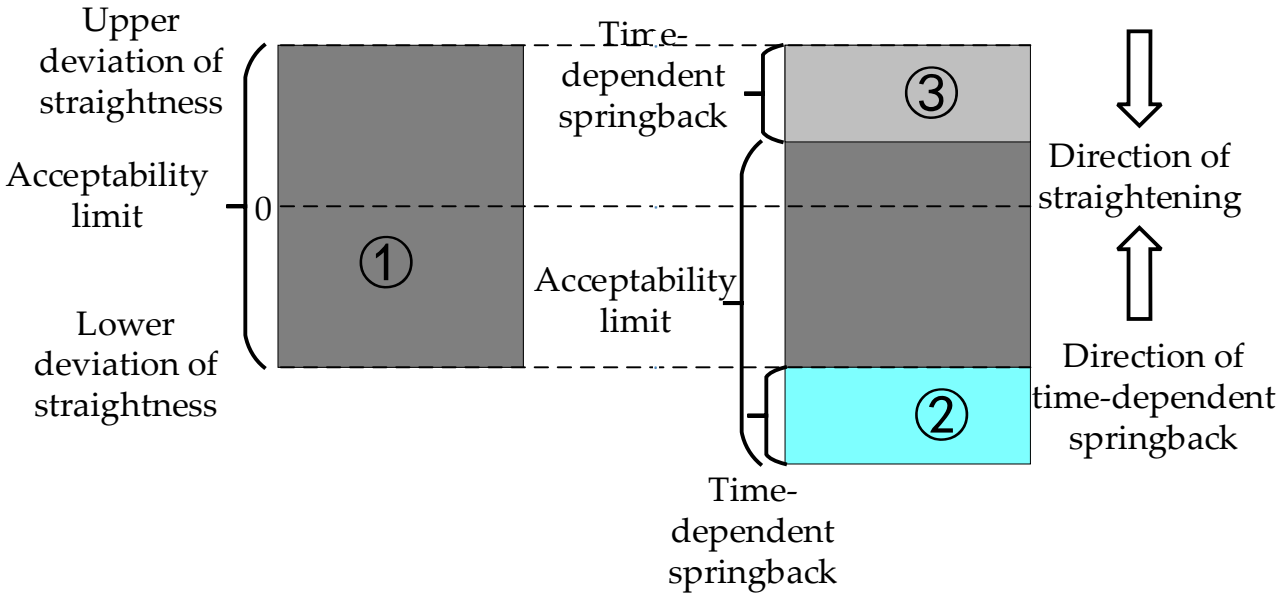


Figure 2. Principles of straightness evaluation and the risk of misjudgment.

Based on the above analysis, the purpose of this paper is to identify the factors affecting time-dependent springback in the process of straightening on the basis of mechanism analysis. We also propose a dynamic straightness-evaluation method considering time-dependent springback. The experimental results show that the genetic algorithm has high prediction accuracy and that the proposed method can effectively reduce the risk of misjudgment.

The innovative work of this paper is as follows: (1) Since there is no relevant research on the phenomenon of time-dependent springback in the process of straightening, there has been no systematic analysis of its influencing factors. So, based on bending-straightening and viscoelastic mechanics, influencing factors affecting time-dependent springback are analyzed on the basis of making certain assumptions. (2) Due to the phenomenon of time-dependent springback, there is a risk of misjudgment in the evaluation of straightness after straightening, so a dynamic evaluation method of straightness is proposed. Based on the GA-BP algorithm, a model to predict the time-dependent springback in straightening is established and compared with the linear regression model. Finally, the dynamic evaluation method of straightness is verified experimentally. (3) In order to explore the contribution of different influencing factors to time-dependent springback, the importance and sensitivity of said factors are analyzed.

The chapters of this paper are arranged as follows: Section 2 analyzes the influencing factors of time-dependent springback in straightening; Section 3 proposes a dynamic evaluation method of straightness based on Section 2; In Section 4, the dynamic evaluation method is verified experimentally; Section 5 analyzes the sensitivity and importance of the influencing factors; Section 6 presents the conclusion.

2. Analysis of Influencing Factors of Time-Dependent Springback Based on Mechanism Analysis

It is worth mentioning that the constitutive model of time-dependent springback is difficult to establish. The purpose of this section is to identify the parameters affecting time-dependent springback as far as possible through mechanism analysis on the premise of making certain assumptions. Thus, we aim to establish a model to quickly predict time-dependent springback based on GA-BP.

Figure 3 shows the Kelvin model, which is used in this paper to analyze the influencing factors of time-dependent springback. E is the elastic modulus of the material, η is the viscosity parameter of the material. σ_0 is the stress of the model, and σ_1 is the stress of the elastic element, and σ_2 is the stress of the viscous element.

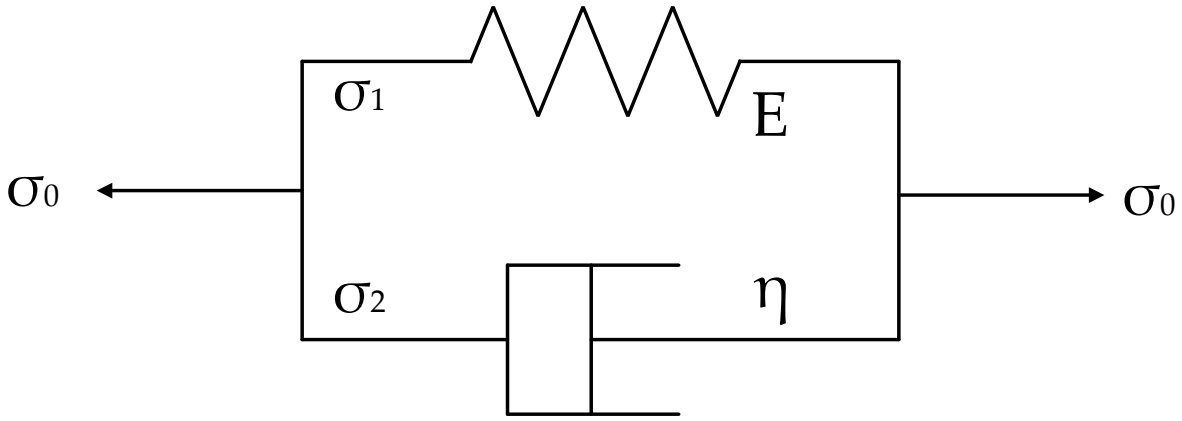


Figure 3. Kelvin model.

Assuming that constant stress $\sigma_0 H(t)$ is loaded at $t = 0$, where t is the time calculated from the loading start time, $H(t)$ is unit step function

$$H(t) = \begin{cases} 1 \; t > 0 \\ 0 \; t < 0 \end{cases} \tag{2}$$

The following relationship exists, where ε is the strain of the model and $\dot{\varepsilon}$ is the strain rate of the model.

$$\sigma_0 = \sigma_1 + \sigma_2 = E\varepsilon + \eta\dot{\varepsilon} \tag{3}$$

The creep model of the Kelvin model can be obtained.

$$\varepsilon(t) = \frac{\sigma_0}{E}\left(1 - e^{-\frac{t}{\tau}}\right) \tag{4}$$

where,

$$\tau = \frac{\eta}{E} \tag{5}$$

The creep compliance $J(t)$ of the Kelvin model can then be obtained.

$$J(t) = \frac{1}{E}\left(1 - e^{-\frac{t}{\tau}}\right) \tag{6}$$

Figure 4 is the schematic diagram of shaft straightening loading.

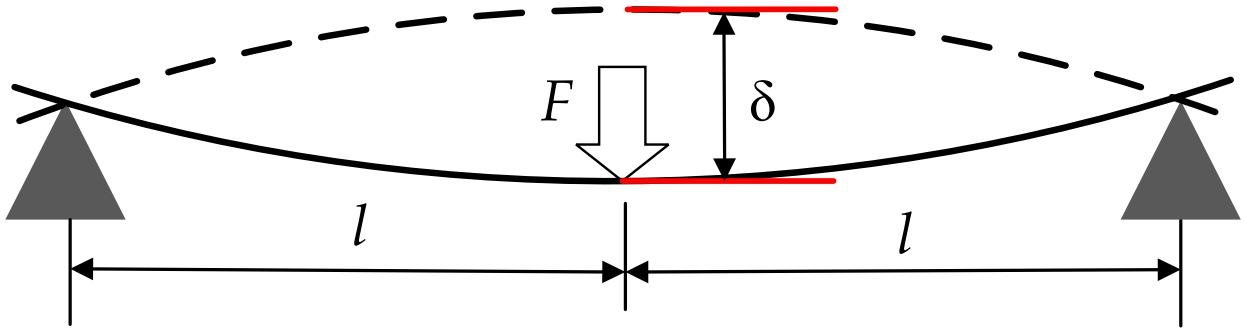


Figure 4. Diagram of straightening load deformation.

When straightening, the load is usually carried in the middle of the two fulcrums. From material mechanics, we know that in the elastic bending stage, the relationship between deflection δ and force F in the middle of the two fulcrums can be expressed as follows:

$$\delta = \frac{Fl^3}{6EI} \tag{7}$$

where I is the inertia moment of the workpiece and l is half the fulcrum distance. According to the corresponding principle of elasticity and viscoelasticity [30], when the shaft is subjected to a step force $F \times H(t)$, the deflection of the shaft can be expressed as follows:

$$\delta = \frac{Fl^3}{6I} J(t) = \frac{Fl^3}{6EI}\left(1 - e^{-\frac{t}{\tau}}\right) \tag{8}$$

Figure 5 shows the changes in force and deflection during the straightening process. δ_C is the straightening stroke and δ_b is instantaneous springback. In the loading stage, the shaft will first undergo elastic bending and then undergo elastic–plastic bending, and then the unloading process is elastic deformation. Phase 1 (loading procedure) can be expressed as follows:

$$F = f_1(\delta) \tag{9}$$

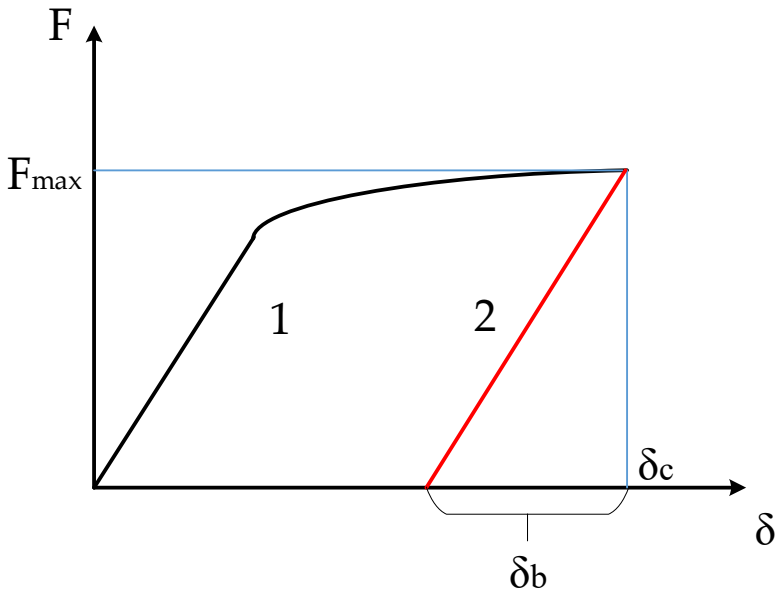


Figure 5. Diagram of force and displacement changes during straightening.

Phase 2 (unloading procedure) can be expressed as follows:

$$F = f_2(\delta) \tag{10}$$

The loading history (Figure 6) of the shaft can be obtained from Phase 1 can be expressed as follows:

$$F = f_1(t) \tag{11}$$

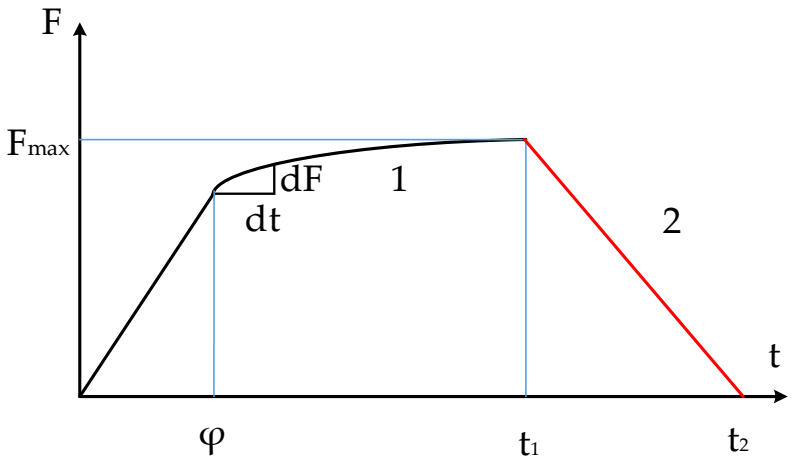


Figure 6. Straightening history diagram of the shaft.

Phase 2 can be expressed as follows:

$$F = f_2(t) \tag{12}$$

If the loading speed of the straightening actuator is v,

$$t = \frac{\delta}{v}\ t_1 = \frac{\delta_C}{v}\ t_2 = \frac{\delta_C + \delta_b}{v} \tag{13}$$

(1) Straightening loading stage

Equation (6) is only suitable for elastic bending, but not for elastic–plastic bending. Due to the complex mechanism of viscous behavior in elastic–plastic bending, in order to analyze the influencing factors, we make the following assumptions:

As shown in Figure 6, t_1 is the end time of straightening loading, and t_2 is the end time of straightening unloading. The force in the loading stage is divided into countless $dF \times H(\varphi)$, and then during the dt period, we think of the shaft as viscoelastic bending, in which the elasticity modulus E and the viscosity coefficient η vary in equal proportion, that is, τ is constant.

According to the Boltzmann accumulate principle [26], we can obtain the following:

$$\begin{aligned} \delta_1(t) = \tfrac{F_0 l^3}{6I} J(t) + \int_0^t \tfrac{l^3}{6I} J(t-\varphi) \times \tfrac{dF}{d\varphi} d\varphi = \\ \tfrac{F_0 l^3}{6EI}\left(1 - e^{-\frac{t}{\tau}}\right) + \int_0^t \tfrac{f'(\varphi) l^3}{6EI}\left(1 - e^{-\frac{t}{\tau}}\right) d\varphi \ 0 < \varphi < t_1 \end{aligned} \tag{14}$$

where $F_0 = f_1(0) = 0$, and

$$\frac{6I}{l^3} \times \frac{1}{J(t)} = \frac{dF}{d\delta} = \frac{dF}{d(v\varphi)} = \frac{dF}{v \times d\varphi} = \frac{f(\varphi)'}{v} \tag{15}$$

Substituting Equation (15) into Equation (14), we can obtain the following:

$$\delta_1(t) = \frac{F_0 l^3}{6EI}\left(1 - e^{-\frac{t}{\tau}}\right) + \int_0^t v\frac{f'(\varphi)}{f'(\varphi)}\left(1 - e^{-\frac{t-\varphi}{\tau}}\right)d\varphi = \int_0^t v\left(1 - e^{-\frac{t-\varphi}{\tau}}\right)d\varphi \; 0 < \varphi < t_1 \tag{16}$$

$$\delta_1(t) = \int_0^t v\left(1 - e^{-\frac{t-\varphi}{\tau}}\right)d\varphi = \delta_C - v\tau\left(e^{\frac{\delta_C}{v\tau}} - 1\right)e^{-\frac{t}{\tau}} \; 0 < \varphi < t_1 \tag{17}$$

where φ is also the time calculated from the loading start time.

(2) Straightening unloading stage

We can think of the unloading phase as reverse loading [31], with the force increasing linearly from 0 to F_{max}. Then, the deflection of straightening unloading stage can be expressed as follows:

$$\delta_2(t) = \int_{t_1}^{t_2} v\frac{f_2(\varphi)'}{f_2(\varphi)'}\left(1 - e^{-\frac{t-\varphi}{\tau}}\right)d\varphi = \int_{\frac{\delta_C}{v}}^{\frac{\delta_C+\delta_b}{v}} v\left(1 - e^{-\frac{t-\varphi}{\tau}}\right)d\varphi t_1 < \varphi < t_2 \tag{18}$$

Therefore, the deflection change throughout the whole straightening process can be expressed as follows:

$$\delta(t) = \delta_2(t) + \delta_1(t) = (\delta_b + \delta_C) - v\tau\left(e^{\frac{\delta_C+\delta_b}{v\tau}} - 1\right)e^{-\frac{t}{\tau}} \; t_2 < t \tag{19}$$

Thus, time-dependent springback can be expressed as follows:

$$\delta(t) - \delta(t_2) = v\tau\left(e^{\frac{\delta_C+\delta_b}{v\tau}} - 1\right)\left(e^{-\frac{\delta_C+\delta_b}{v\tau}} - e^{-\frac{t}{\tau}}\right) \; t_2 < t \tag{20}$$

However, there is a problem. Since the time-dependent springback analytical model is derived according to the creep model, during the straightening process of loading, we control the displacement of the straightening actuator precisely, which will inevitably generate errors. At the same time, the derivation process of the model also made some assumptions. Considering the effect of error compensation, we use Equation (21) to express time-dependent springback.

$$\delta(t) - \delta(0) = v\tau\left(e^{\frac{\delta_C+\delta_b}{v\tau}} - 1\right)\left(1 - e^{-\frac{t}{\tau}}\right) \tag{21}$$

When evaluating straightness, we focus on the time-dependent springback after saturation, not the springback process itself. When $t \to \propto$, δ_{ts} is the saturation time-dependent springback.

$$\delta_{ts} = v\tau\left(e^{\frac{\delta_C+\delta_b}{v\tau}} - 1\right) \tag{22}$$

It can be seen from Equation (22) that, on the premise that the loading history of the straightening is determined, time-dependent springback is related to the straightening actuator speed v, straightening stroke δ_C, unloading stroke δ_b, and viscoelastic parameter τ. The straightening actuator speed v is related to the straightening time (time of the shaft-bending deformation process), t_s. Therefore, we can preliminarily screen out the three influencing factors δ_C, δ_b, and t_s.

According to the bending-straightening theoretical model [2,32], material parameters and fulcrum distance L will affect the loading history of straightening. As can be seen between Equations (7) and (12), τ also affects the straightening loading history. As shown in Figure 6, the straightening loading history is closely related to force and t_s.

Since material parameters cannot be obtained in real time, but related physical parameters affected by material parameters can be, after comprehensive evaluation, in order to establish the fast prediction model of time-dependent springback, the following are selected as the influencing factors: δ_C, δ_b, t_s, L, and F_{max}.

3. Dynamic Method for Evaluation of Straightness Considering Time-Dependent Springback

3.1. Principle of Method for Dynamic Evaluation of Straightness

Based on the above analysis, a method for the dynamic evaluation of straightness is proposed.

Figure 7 shows the structure of the straightening actuator of the self-made straightening machine. The pressure head can detect separation and contact with the shaft, the force sensor can detect the straightening force in real-time, and the grating ruler can detect the displacement of the pressure head. The grating displacement sensor collects data on time-dependent springback, and it does not exist in the normal straightening process.

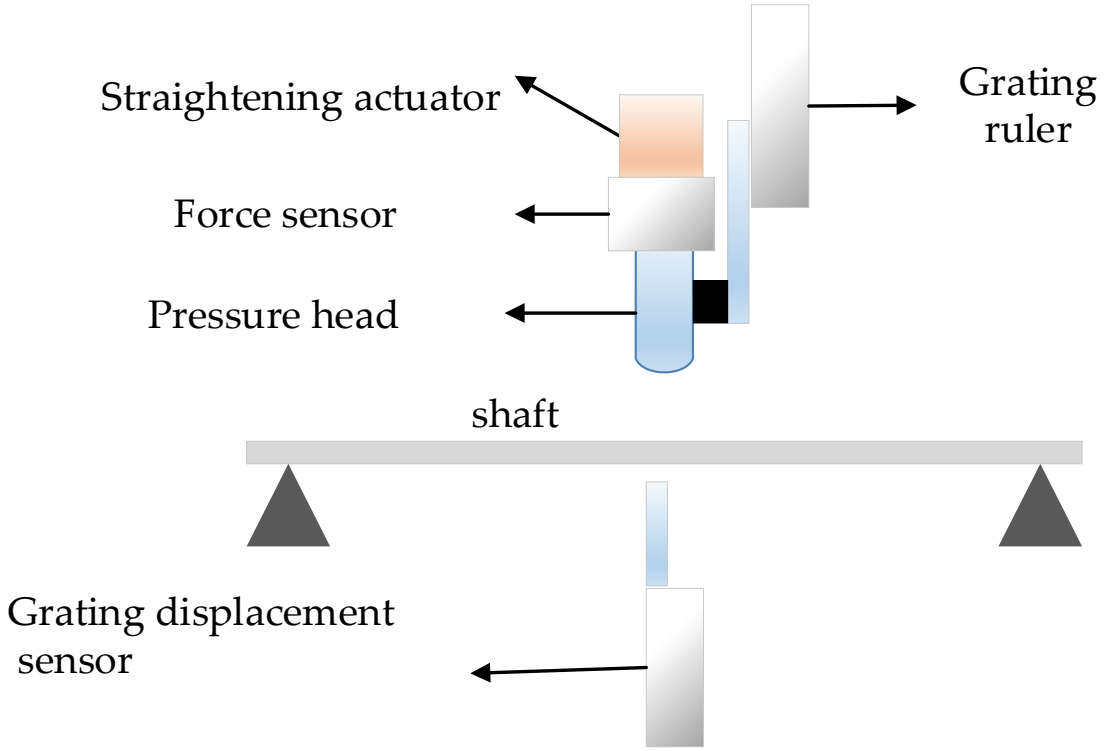


Figure 7. Self-made straightening equipment and experimental equipment.

As shown in Figure 8a, during straightening, the pressure head first detects contact with the shaft. At this time, the system records the position information S_1 of the grating ruler and time t_0. When the straightening load is complete, the system records the position information S_2 of the grating ruler and time t_1, as well as the force value F_{max}. Then, straightening and unloading begin, and when the pressure head is determined to be separated from the shaft, the system records the position information S_3 of the grating ruler and time t_2.

These parameters can be obtained in real-time. At this point, as shown in Figure 8b, the influencing factors analyzed in Section 2 are taken as input in real-time, and saturation time-dependent springback δ_{ts} is predicted through the prediction model of time-dependent springback in real-time. Then, the acceptability limit of straightness can be directly obtained as follows:

$$(\text{Upper deviation of straightnes(Ud)} - \delta_{ts}, \text{Lower deviation of straightness(Ld)} - \delta_{ts}).$$

The control system can then evaluate the straightening effect according to the acceptability limit in real-time. Therefore, the most critical problem is establishing the prediction model of time-dependent springback.

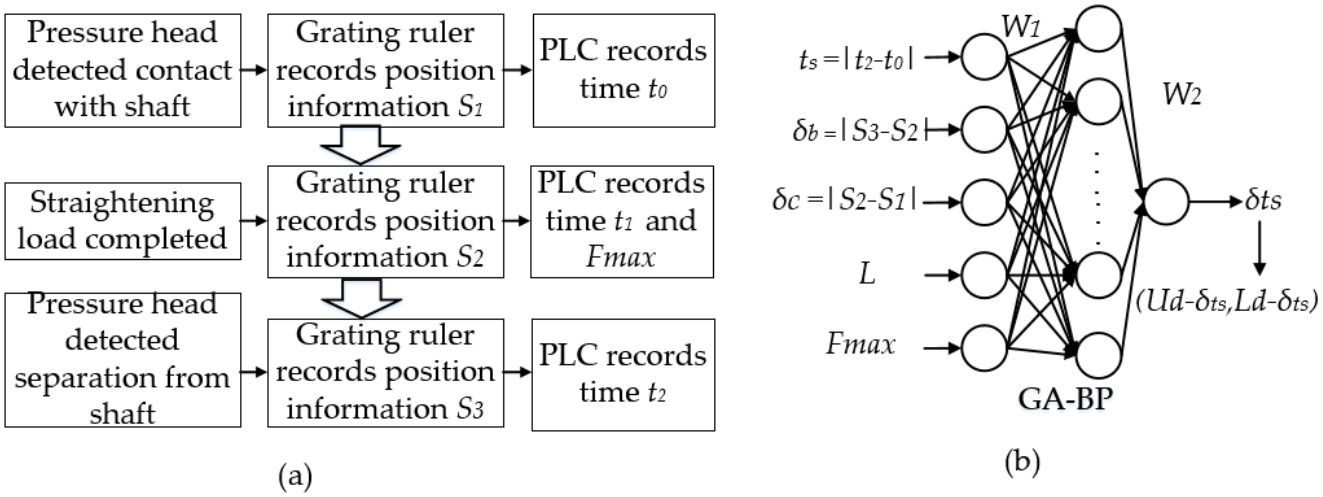


Figure 8. (**a**) Data collection strategies for input variables; (**b**) The prediction model of the dynamic acceptability limit of straightness.

3.2. Time-Dependent-Springback Prediction Model Based on GA-BP Neural Network

3.2.1. BP Neural Network Prediction Model

The BP neural network is a typical feedforward neural network, which can approximate the nonlinear continuous functions with arbitrary precision. In this paper, a three-layer (including input layer) neural network is selected to establish the prediction model. According to the previous analysis, there are five main parameters that affect time-dependent springback. Therefore, there are five nodes in the input layer, namely, straightening stroke δ_C, straightening force F_{max}, straightening time t_s, fulcrum distance L, and instantaneous springback stroke δ_b. The output is saturated with time-dependent springback δ_{ts}.

The transfer function between the input layer and the hidden layer adopts a sigmoid function. This is expressed as follows:

$$f_1(x) = \frac{e^x - e^{-x}}{e^x + e^{-x}} \tag{23}$$

The transfer function between the output layer and the hidden layer adopts a purelin function. This expressed as follows:

$$f_2(x) = x \tag{24}$$

Therefore, the prediction model can be expressed as follows:

$$\delta_{ts} = f_2\left\{w_2 \times f_1\left[w_1 \times (t_s, \delta_b, \delta_C, L, F_{max})^T + b_1\right] + b_2\right\} \tag{25}$$

where w_1 is the weight matrix from the input layer to the hidden layer, w_2 is the weight matrix from the hidden layer to the output layer, and b_1 and b_2 are threshold matrices of the hidden layer and output layer.

The number of nodes in the hidden layer has an important influence on the performance of the prediction model, and there is no relevant theory regarding the selection of the number of nodes in the hidden layer. The selection can be based on empirical formulas.

$$\begin{cases} h = \sqrt{m+n} + a \\ h = \log_2 m \\ h = \sqrt{mn} \end{cases} \tag{26}$$

where h, m and n are the number of nodes in the hidden layer, the number of nodes in the input layer, and the number of nodes in the output layer, respectively, and a is a constant from 1 to 10. Thus, the number of nodes of the hidden layer is 3–13.

In this paper, the performance evaluation function of the BP neural network is the root mean square error (RMSE). The maximum number of training points is 1000, and the learning rate is 0.01, setting the training accuracy at 0.001. The Levenberg–Marquardt algorithm is used for network training.

However, the BP neural network also has disadvantages, including the fact that the weight and deviation of the network easily fall into the local minimum value, and there is no possibility for global searching. Thus, this paper uses the genetic algorithm (GA) to optimize the BP neural network.

3.2.2. BP Neural Network was Optimized by GA

The genetic algorithm (GA) simulates the genetic evolution process of organisms in nature and has the advantage of global searching for optimal values, which can make up for the disadvantage of the BP neural network in terms of easily falling into a local minimum value. The process of BP neural network optimization by GA is shown in Figure 9.

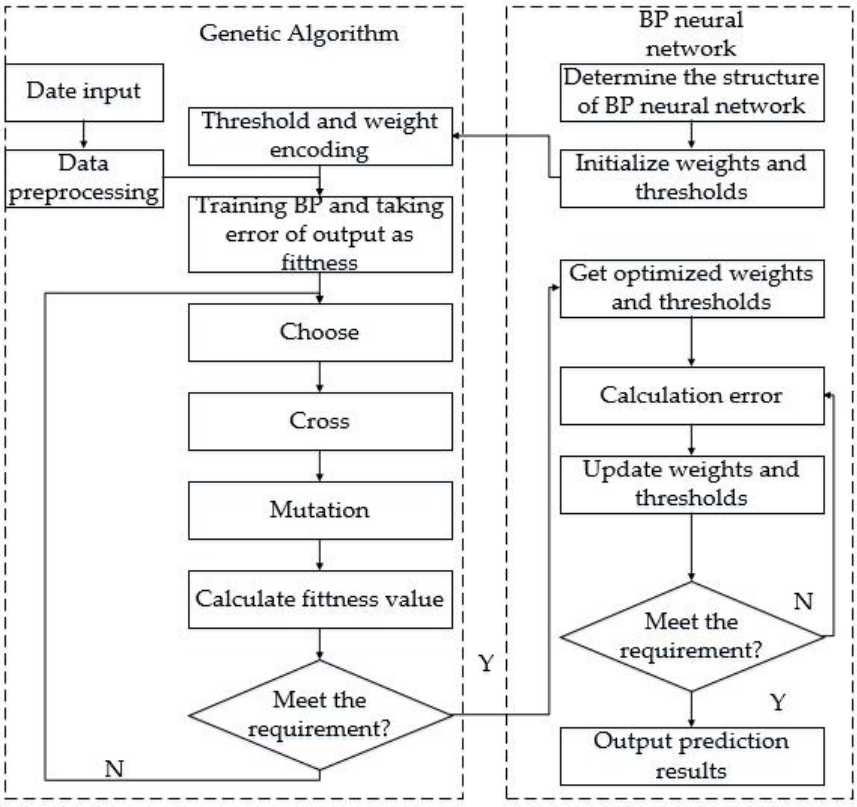


Figure 9. Optimization process of BP neural network by genetic algorithm.

1. Firstly, the structure of the BP neural network is determined;
2. The population is initialized, and then the weights and thresholds of the BP neural network are coded;
3. Populations are selected, crossed, and mutated;
4. The fitness values, f are calculated to determine the fitness of individuals in a population. In this paper, the root mean square error (RMSE) of the predicted output and

the target output of the BP neural network is selected as the fitness function, and the calculation formula is as follows: $\hat{y}_i$ is target output, y_i is prediction output;

$$f = \sqrt{\frac{1}{n}\sum_{i}^{n}(y_i - \hat{y}_i)^2} \tag{27}$$

5. We judge whether the stop condition of the GA algorithm is met. If so, the weight and threshold values after optimization are passed to the BP neural network. If the stop condition is not met, steps 3–5 is repeated.

3.3. Experimental Data Collection

In this paper, the shaft, which is commonly used by relevant enterprises, is a regular hexagonal section shaft; the maximum inner circle diameter is 12 mm; the material is 304 stainless steel.

As shown in Figure 7, in order to collect data on time-dependent springback, a grating displacement sensor is placed at the midpoint of two fulcrum points below the shaft, and the displacement information on the grating displacement sensor is collected as soon as the shaft is separated from the pressure head. The resolution of the displacement sensor is 0.001 mm, and the uncertainty is ±0.3 μm.

In the process of bending forming, the greater the bending angle of the titanium tube, the greater the time-dependent springback angle, and the longer the saturation time of the time-dependent springback [15]. Thus, in the straightening process, the greater the straightening stroke δ_C, the greater the time-dependent springback and the longer the saturation time. Therefore, in order to determine the saturation time, the straightening speed was 20 mm/s, the fulcrum distance L = 665 mm, and the straightening of the stroke was 30 mm. The experimental results are shown in Figure 10.

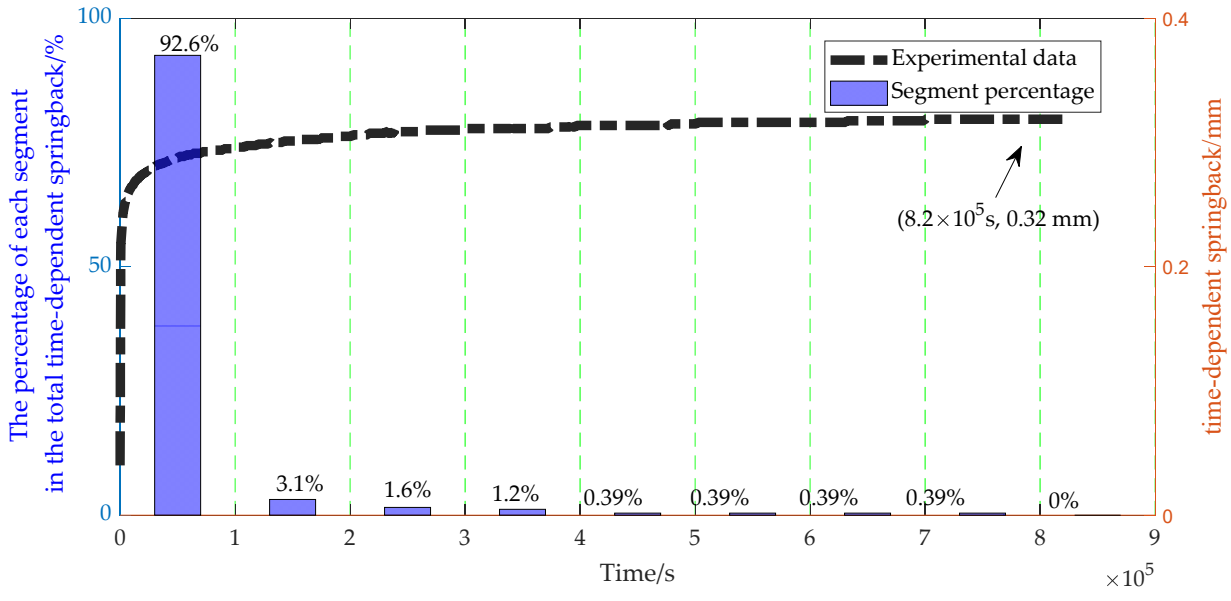


Figure 10. Time-dependent springback experimental data of 10 days.

It can be seen that after 10 days of data collection, the time-dependent springback essentially reaches saturation, and the small springback amount after that has no great significance to engineering applications. Therefore, we chose 10 days as the saturation time for time-dependent springback.

In order to save time during data collection, we performed curve fitting on the data of the first 4 h from Figure 10 to predict the saturation data after 10 days. Figure 11 shows the predicted results.

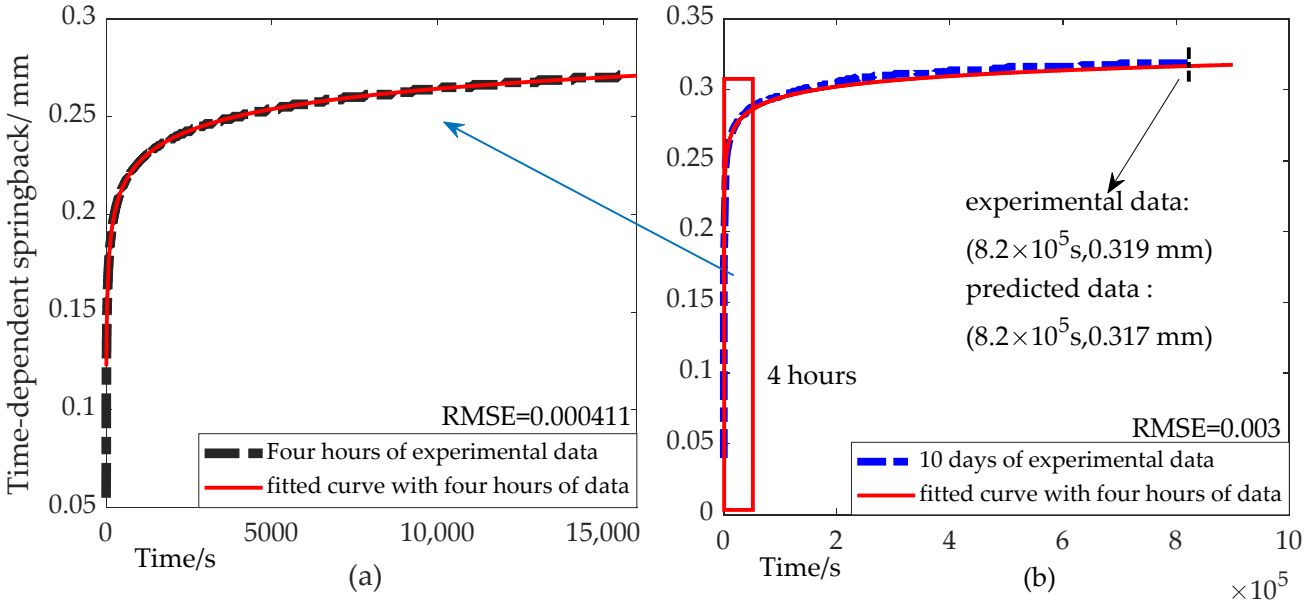


Figure 11. (**a**) Curve fitting using four hours of experimental data; (**b**) Use the fitting curve to predict the data ten days later.

The fitting curve was compared with the experimental data of 10 days, and the root mean square error (RMSE) was calculated as follows:

$$\mathrm{RMSE} = \sqrt{\frac{\sum_{i=1}^{n}\left(y_{experiment} - y_{predicted}\right)^2}{n}} \tag{28}$$

where $y_{experiment}$ is the experimental value and $y_{predicted}$ is the predicted value.

After calculation, the RMSE of the curve fitted with the 4-h experimental data and the 10-day experimental data is 0.003 mm. The saturation data predicted by the curve fitting after 10 days is 0.317 mm, which is only 0.002 mm different from the experimental value of 0.319 mm. Therefore, in this paper, in order to save on the cost of data collection, only 4 h of data were collected, and then MATLAB was used for curve fitting to predict saturation data.

In our straightening equipment, the fulcrum distances are fixed at 475 mm, 570 mm, 665 mm, and 760 mm. Therefore, under the condition that the straightening speed is 20 mm/s, the saturated time-dependent springback data (Tables 1–4) are obtained by changing the straightening stroke δ_C as follows:

Table 1. Experimental results of fulcrum distance: 475 mm.

δ_C/mm	F_{max}/N	t_s/s	δ_b/mm	L	δ_{ts}/mm
3.899	417	0.39	3.870	475	0.02
5.880	630	0.59	5.845	475	0.028
7.858	839	0.78	7.787	475	0.04
9.824	1035	0.97	9.604	475	0.056
11.816	1216	1.16	11.285	475	0.087
13.79	1372	1.33	12.735	475	0.119
15.781	1503	1.47	13.944	475	0.144
17.679	1603	1.63	14.868	475	0.173

Table 2. Experimental results of fulcrum distance: 570 mm.

δ_C/mm	F_{max}/N	t_s/s	δ_b/mm	L	δ_{ts}/mm
4.879	302	0.49	4.849	570	0.0205
7.843	480	0.78	7.692	570	0.0406
9.804	597	0.97	9.567	570	0.0450
11.768	711	1.16	11.402	570	0.094
13.735	819	1.34	13.121	570	0.128
15.692	913	1.52	14.640	570	0.154
17.677	1002	1.69	16.060	570	0.196
19.643	1080	1.85	17.312	570	0.217

Table 3. Experimental results of fulcrum distance: 665 mm.

δ_C/mm	F_{max}/N	t_s/s	δ_b/mm	L	δ_{ts}/mm
5.976	235	0.6	5.975	665	0.033
8.001	311	0.8	7.921	665	0.041
9.965	384	0.99	9.774	665	0.072
11.970	457	1.18	11.641	665	0.089
13.952	529	1.37	13.460	665	0.120
15.951	600	1.56	15.270	665	0.135
17.971	670	1.75	17.055	665	0.155
19.935	736	1.93	18.723	665	0.187

Table 4. Experimental results of fulcrum distance: 760 mm.

δ_C/mm	F_{max}/N	t_s/s	δ_b/mm	L	δ_{ts}/mm
6.474	170	0.65	6.473	760	0.039
8.449	221	0.84	8.397	760	0.053
10.425	271	1.04	10.311	760	0.075
12.372	320	1.23	12.162	760	0.093
14.336	369	1.42	14.007	760	0.110
16.295	416	1.61	15.814	760	0.146
18.269	463	1.8	17.604	760	0.182
20.247	509	1.98	19.356	760	0.205

3.4. The Establishment of Time-Dependent Springback Prediction Model

A total of 32 groups of experimental data were collected, among which 4 groups of data (Table 5) were used as test sets to verify the generalization ability of the model.

Table 5. Test set data.

δ_C/mm	F/N	t/s	δ_b/mm	L	δ_{ts}/mm	δ_{ts_prd}/mm	Error/mm	$\lvert\frac{Error}{\delta_t}\rvert$/%
9.824	1035	0.97	9.604	475	0.056	0.0567	0.0007	0.012
15.692	913	1.52	14.64	570	0.154	0.1552	0.0012	0.008
17.971	670	1.75	17.055	665	0.155	0.157	0.002	0.013
14.336	369	1.42	14.007	760	0.11	0.1138	0.0038	0.035

Before model training, data needed to be normalized. The normalization process was carried out according to the following formula:

$$X_0 = \frac{X - X_{min}}{X_{max} - X_{min}} \tag{29}$$

where X_0 is the normalized value, X are the experimental data, X_{min} is the minimum value of the experimental data, and X_{max} is the maximum value of the experimental data.

After extensive testing, the number of nodes in the hidden layer is finally determined to be 8, so the structure of the BP neural network in this paper is 5-8-1.

The individual coding length of the genetic algorithm is $5 \times 8 + 8 + 9 = 57$, the population number is 20, the crossover rate is 0.4, the mutation rate is 0.1, and the number of iterations is 200.

Figure 12 shows the iterative process of the genetic algorithm. In around the 20th generation, the optimal interval between the weight and threshold value of the BP neural network is found. It can be seen that the genetic algorithm is able to continuously optimize the BP neural network, and it can compensate for the BP neural network's disadvantage of easily falling into a local minimum value. Then, the weights and thresholds are transferred to the BP neural network for model training.

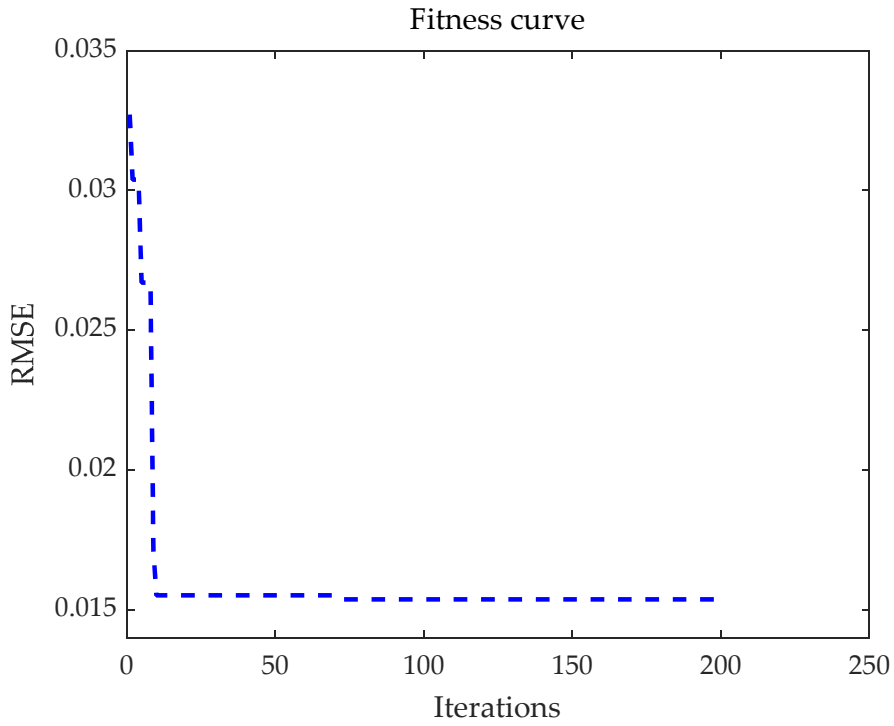


Figure 12. Iterative process of genetic algorithm.

Figure 13 shows the training results of the BP neural network optimized by the genetic algorithm, and the regression value, R, represents the correlation between the output results and target values.

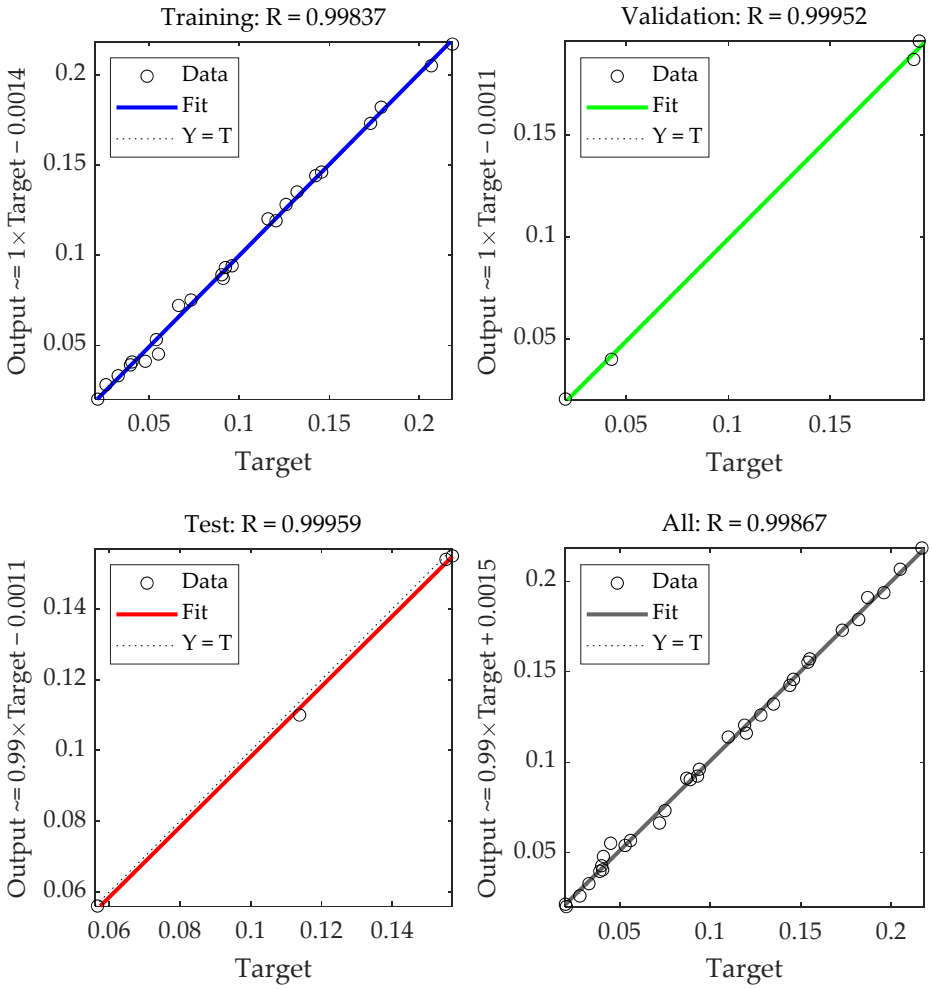


Figure 13. GA-BP Neural Network training regression.

The regression values, R, of the training, verification, and test sets were 0.99837, 0.99952, and 0.99959, respectively, and the regression value of the whole set was 0.99867. This indicates that the correlation between the output value and the target value is high and that the model is good.

Figure 14 shows the predicted and target values of the test set. They almost coincide. Figure 15 shows the error between the target value and the prediction value, and Figure 16 shows the percentage error against the target value. As can be seen from the figure, among the four groups of test data, the maximum error is 0.0038 mm, and the maximum error percentage is 0.035%. This shows that the BP neural network optimized by the genetic algorithm has good generalization ability and high prediction accuracy.

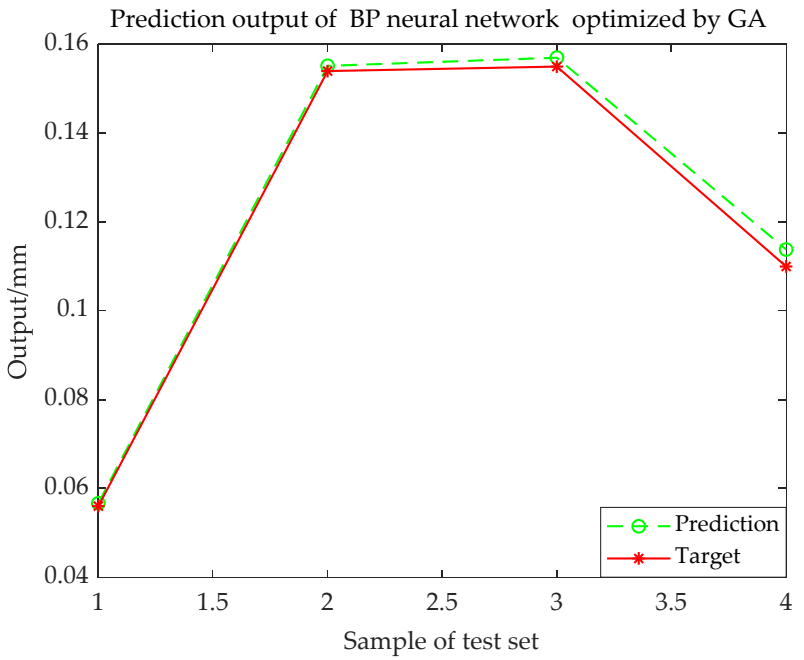


Figure 14. Predicted values of GA-BP and experimental values.

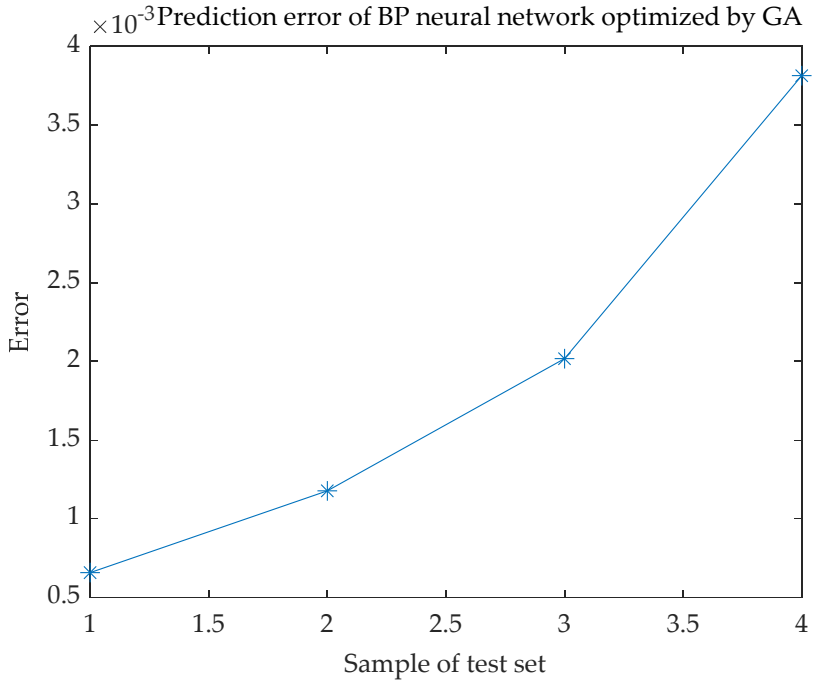


Figure 15. Error between predicted value of GA-BP and experimental value.

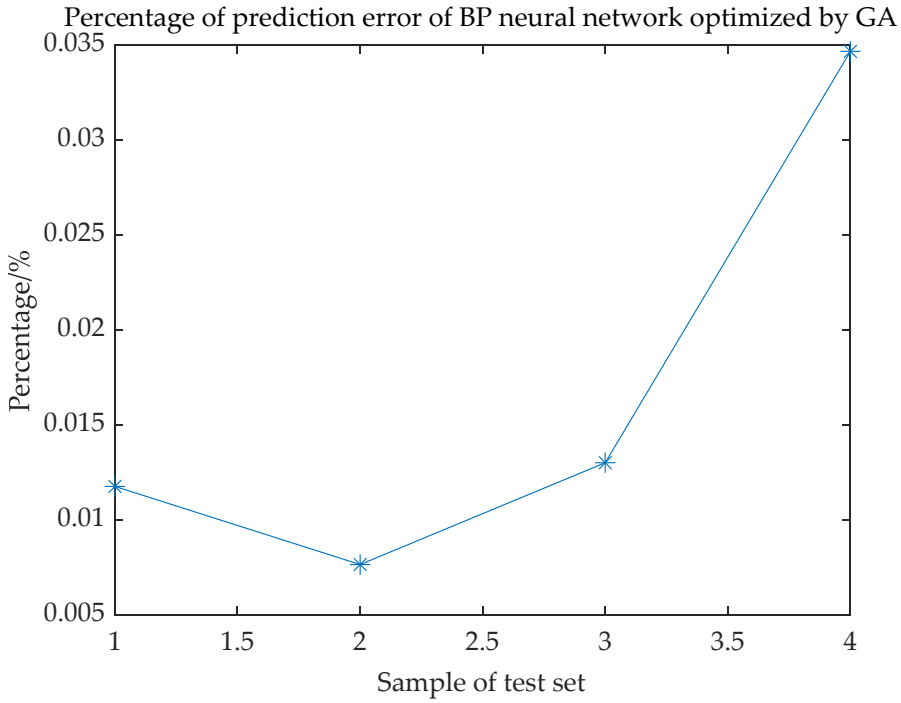


Figure 16. Percentage of error between predicted value of GA-BP and experimental value.

3.5. Prediction Model Comparison

In order to further compare the performances of the prediction models, a multiple linear regression model was used to calculate the predicted values of the test sets. Using data from the training set and validation set for fitting, the regression model is shown in Equation (30). The degree of fit (R^2) was 0.9759.

$$\delta_{ts} = 0.0101 + 0.00864 \times \delta_C - 0.00004 \times F_{max} + 0.49862 \times t - 0.04691 \times \delta_b - 0.000068 \times L \quad (30)$$

The regression model was used to predict the test set data, and the prediction error and GA-BP model prediction error are plotted in Figure 17. As can be seen from the figure, the prediction accuracy of the GA-BP model is much higher than that of the regression model. The maximum prediction error of the regression model is 0.014 mm, with a maximum error percentage of 0.127%, much higher than that of the GA-BP model. The RMSE and degree of fit (R^2) are used to further evaluate the accuracy of the prediction models. The formula for R^2 is as follows:

$$R^2 = 1 - \frac{\sum_{i=1}^{n}(y_1 - y_2)^2}{\sum_{i=1}^{n}(y_1 - \overline{y_1})^2} \quad (31)$$

where y_1 is the target value, y_2 is the prediction value, $\overline{y_1}$ is the average of the target value. Two evaluation indexes were calculated using test set data.

As shown in Table 6, the RMSE of the GA-BP model is 0.0042, and that of the regression model is 0.0098. The R^2 of the GA-BP model is 0.9969 and that of the regression model is 0.9416. This shows that the relationship between input variables and output variables is not a simple linear relationship but a more complex nonlinear one. Furthermore, the GA-BP neural network has a good nonlinear fitting ability; it can learn the complex relationship between variables and is more suitable for the prediction of time-dependent springback in straightening.

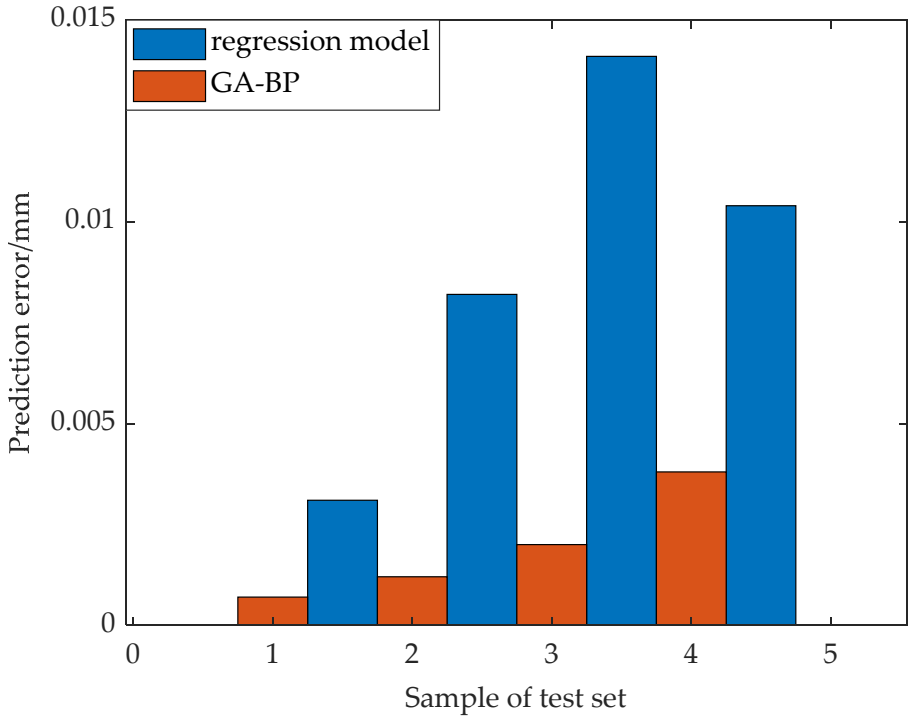


Figure 17. Comparison of prediction error between GA-BP model and regression model.

Table 6. RMSE and R^2 of two prediction models.

	RMSE	R^2
GA-BP	0.0042	0.9969
regression model	0.0098	0.9416

At the same time, it also shows that the influencing factors screened in Chapter 2 can better predict the time-dependent springback. The model is successful.

4. Experimental Verification of Dynamic Evaluation Method of Straightness

In order to verify the effectiveness of the proposed method for the dynamic evaluation of straightness, an experiment was carried out on self-made straightening equipment. Through the method proposed in Section 3, data were collected in real-time during the straightening process, and the GA-BP model was used to predict the saturated time-dependent springback in real-time. Then, the acceptability limits of straightness were calculated to dynamically evaluate the straightness after straightening.

Two groups of experiments were carried out. The fulcrum distance was 760 mm, and the straightening speed was 20 mm/s. The straightness error requirement is 0.15 mm/760 mm.

Experimental data are shown in Table 7. Straightness is measured immediately after straightening, and then the dynamic evaluation method of straightness is used to evaluate straightness. Then, 10 days later, the straightness of the shaft was measured again to check whether the straightness was consistent with the results of the dynamic evaluation method, so as to verify its effectiveness.

Table 7. Experiment result.

Number	F/N	t_s/s	δ_C/mm	δ_b/mm
1	368	1.4	14.34	14.007
2	463	1.8	18.27	17.604
Straightness error/mm	**Predicted δ_{ts}/mm**	**Evaluation result**		**Straightness error after 10 days/mm**
0.134	0.121	No pass		0.261
−0.251	0.168	Pass		−0.075

Figure 18 shows the acceptability limits of two groups of experiments. It can be seen from Table 6 that the straightness error of the first shaft is located in the range ③, and the system judged that the straightness error was unqualified. Ten days later, the straightness error was measured again, and it was 0.261 mm/760 mm. Obviously, the straightness error of the shaft did not meet the requirements of straightness. The second shaft is located in range ②. Although the straightness error is −0.251 mm/760 mm, the system judged it to be qualified. Ten days later, the straightness error was measured again, and it was −0.075 mm/760 mm, meeting the requirement for straightness.

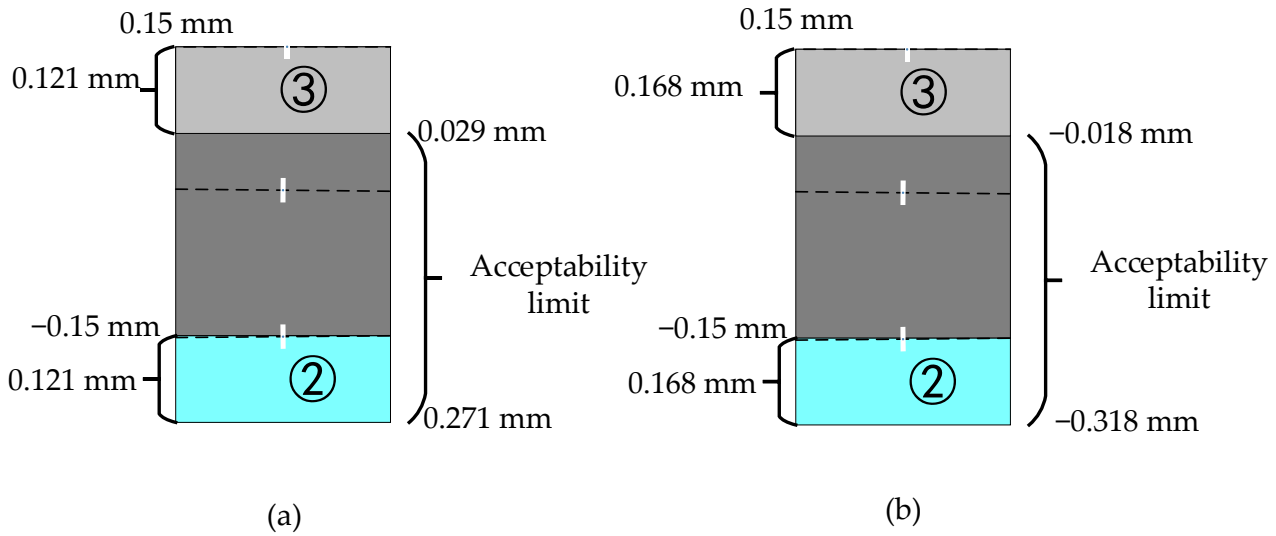


Figure 18. (**a**) Acceptability limit after dynamic adjustment for shaft 1; (**b**) Acceptability limit after dynamic adjustment for shaft 2.

This proves that the dynamic evaluation method of straightness considering time-dependent springback proposed in this paper is effective, which can improve the quality of straightness detection and effectively reduce the risk of misjudgment.

5. Discussion

5.1. The Sensitivity and Relative Importance of Input Variables

In this paper, the prediction method based on the GA-BP neural network is used to dynamically evaluate straightness. There are five inputs, and each input has a varying influence on the output. In order to explore the sensitivity and relative importance of the

input variables, the weight of the neural network and the Garson equation [33,34] is used to evaluate each variable. The calculation formula is as follows:

$$I_j = \frac{\sum_{m=1}^{N_h}\left(\left(\frac{\left|w_{jm}^{ih}\right|}{\sum_{k=1}^{N_i}\left|w_{km}^{ih}\right|}\right)\times\left|w_{mn}^{ho}\right|\right)}{\sum_{k=1}^{N_i}\left\{\sum_{m=1}^{N_h}\left(\left(\frac{\left|w_{jm}^{ih}\right|}{\sum_{k=1}^{N_i}\left|w_{km}^{ih}\right|}\right)\times\left|w_{mn}^{ho}\right|\right)\right\}} \tag{32}$$

where, I_j is the importance of the jth input. N_i, N_h are the number of nodes of the input and hidden layers, respectively; w is the weight; i, h, o represent the input layer, hidden layer, and output layer, respectively.

The weight matrix is derived from the established GA-BP model, and then Equation (30) is used to calculate the sensitivity and relative importance of the input. The calculation results are shown in Figure 19.

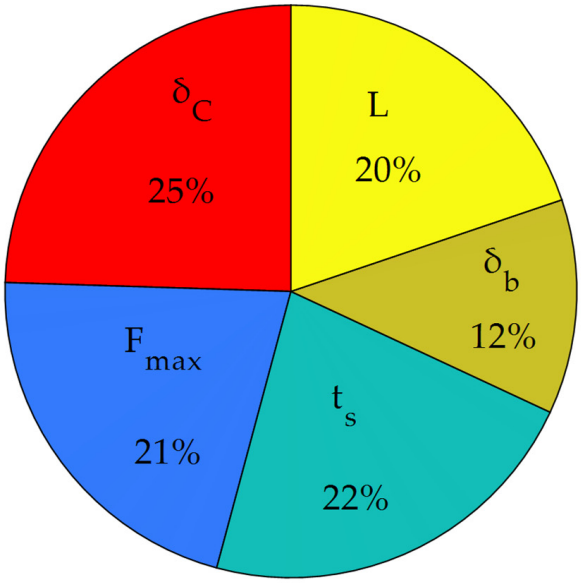


Figure 19. Sensitivity and relative importance of input variables.

As can be seen, each input variable has relatively high degrees of importance and sensitivity. The straightening stroke δ_C has the greatest impact, at 25%; second is the straightening time t_s, which is 22%; followed by the straightening force F_{max}, which is 21%; the fulcrum distance L, which is 20%; finally, instantaneous rebound δ_b, with low sensitivity and relative importance, is 12%. Thus, the order is $\delta_C > t_s > F_{max} > L > \delta_b$.

5.2. Discussion on Elasto-Viscoplastic Model

We discuss whether the elasto-viscoplastic model is suitable for analyzing the factors affecting time-dependent springback during the straightening process. The elasto-viscoplastic model can be represented by a spring and a Bingham model, as shown in Figure 20.

When the stress σ of the model is less than the yield stress σ_s, the elasto-viscoplastic model has only elastic deformation. When the stress σ of the model is greater than the yield stress σ_s of the material, the Bingham model begins to produce plastic deformation and viscous properties begin to appear.

Let us consider the straightening process. It is a continuous process, divided into loading and unloading phases. Unloading is an elastic process, and the bending moment of the workpiece is zero after unloading. According to the straightening theory, straightening is directly related to small deformation, and the workpiece will not reverse yield after unloading [32]. That is, the stress σ inside the workpiece is less than the yield stress σ_s.

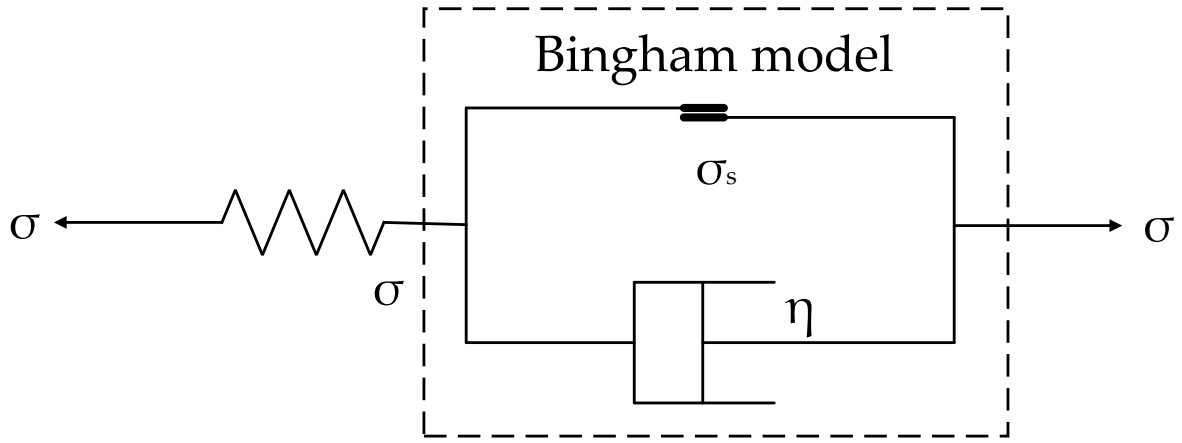


Figure 20. Elasto-viscoplastic model.

In this sense, the elasto-viscoplastic model does not seem to capture the viscosity effect after straightening unloading. We chose a simpler and more suitable viscoelastic model to analyze the influencing factors of time-dependent springback in the straightening process, and it has a good effect.

5.3. Effect of Springback on Straightening Speed

To assure straightening efficiency, straightening is usually evaluated immediately after straightening. Due to the existence of time-dependent springback, the straightness of the workpiece changes with the time-dependent springback after straightening. By proposing a dynamic evaluation method of straightness considering time-dependent springback, straightness can be evaluated immediately after straightening, avoiding the influence of time-dependent springback on the straightening speed.

6. Conclusions

In view of the presence of time-dependent springback in straightening, a method for dynamic evaluation of straightness considering this phenomenon is proposed in this paper. In view of the lack of relevant studies on this topic, this paper analyzes the factors influencing this phenomenon on the premise of making certain assumptions based on viscoelastic mechanics and bending-straightening. This way, we established a fast prediction model for time-dependent springback. Because the constitutive model is difficult to establish and no one has used machine-learning to predict the time-dependent springback in straightening before now, this paper uses the GA-BP algorithm to establish a prediction model, providing a new idea for research within this field. Then, the effectiveness of the method for dynamic evaluation of straightness considering time-dependent springback is verified experimentally. Finally, the sensitivity and relative importance of the influencing factors are analyzed. The following conclusions are drawn:

(1) The influencing factors of time-dependent springback in the straightening process include straightening stroke δ_C, fulcrum distance L, straightening time t_s, straightening force F_{max}, and instantaneous springback δ_b. These parameters can be used as the main influencing factors to establish the prediction model of time-dependent springback;

(2) Based on the GA-BP neural network and taking parameters in conclusion 1 as input, the time-dependent springback prediction model has high prediction accuracy, with a maximum error of 0.0038 mm, a maximum relative error of 0.035%, and a RMSE of 0.0042, which are far lower than those for the linear regression model. The R^2 of the GA-BP, 0.9969, is also better than that of the linear regression model. This indicates that the influencing factors from Conclusion 1 are accurate enough to predict time-dependent springback and can be used in practical applications;

(3) The experimental results show that the proposed method can effectively reduce the two kinds of risks;
(4) Conclusion 1 mentioned the influencing factors of time-dependent springback. Their relative importance and sensitivity are in the order of $\delta_C > t_s > F_{max} > L > \delta_b$.

The influence of the time-dependent springback phenomenon in the straightening process is not only reflected in the evaluation of straightness but also in the calculation of straightening stroke. This is the key problem to be solved in our next work.

Author Contributions: Conceptualization, methodology, supervision, project administration, funding acquisition, Z.Y.; software, validation, writing—original draft preparation, writing—review and editing, Q.K. All authors have read and agreed to the published version of the manuscript.

Funding: This research was supported by the National Natural Science Foundation of China (Grant No. 51675481).

Institutional Review Board Statement: Not applicable.

Informed Consent Statement: Not applicable.

Data Availability Statement: Not applicable.

Conflicts of Interest: The authors declare no conflict of interest.

References

1. Samuel, G.L.; Shunmugam, M.S. Evaluation of straightness and flatness error using computational geometric techniques. *Comput.-Aided Des.* **1999**, *31*, 829–843. [CrossRef]
2. Lu, H.; Ling, H.; Leopold, J.; Zhang, X.; Guo, C. Improvement on straightness of metal bar based on straightening stroke-deflection model. *Sci. China Ser. E Technol. Sci.* **2009**, *52*, 1866–1873. [CrossRef]
3. Yuz, H.; Zhou, L.J. Key technologies of vertical press-straightening of elevator rail. *J. Zhejiang Univ.* **2010**, *44*, 1502–1507. Available online: https://kns.cnki.net/kcms/detail/detail.aspx?dbcode=CJFD&dbname=CJFD2010&filename=ZDZC201008017&uniplatform=NZKPT&v=Hfunx7XwgYB68JfbbqRa2x-IdWMtMVmxmuxvpIbguS4edI_GXJe-9YXZFhIXEb2_ (accessed on 12 April 2022).
4. Pei, Y.C.; Wang, J.W.; Tan, Q.C.; Yuan, D.-Z.; Zhang, F. An investigation on the bending straightening process of D-type cross section shaft. *Int. J. Mech. Sci.* **2017**, *131*, 1082–1091. [CrossRef]
5. Hong, L.; Xiong, X. Research on straightening process model based on iteration and self-learning. In Proceedings of the 2016 IEEE 11th Conference on Industrial Electronics and Applications (ICIEA), Hefei, China, 5–7 June 2016; pp. 2400–2406.
6. Li, J.; Zou, H.; Xiong, G.L. Establishment and Application of Load-Deflection Model of Press Straightening. In *Key Engineering Materials*; Trans Tech Publications, Ltd.: Bäch, Switzerland, 2004; Volume 274, pp. 475–480. [CrossRef]
7. Zhao, J.; Song, X. Control strategy of multi-point bending one-off straightening process for LSAW pipes. *Int. J. Adv. Manuf. Technol.* **2014**, *72*, 1615–1624. [CrossRef]
8. Mao, H.; Li, Z.; Lan, J.; Chen, H.; Zhang, B. Three-point bending straightening algorithm and verification for I-type seamless welded rail. *Proc. Inst. Mech. Eng. Part B J. Eng. Manuf.* **2021**, 09544054211060915. Available online: https://journals.sagepub.com/doi/abs/10.1177/09544054211060915 (accessed on 12 April 2022). [CrossRef]
9. Lim, H.; Lee, M.G.; Sung, J.H.; Kim, J.; Wagoner, R. Time-dependent springback of advanced high strength steels. *Int. J. Plast.* **2012**, *29*, 42–59. [CrossRef]
10. Sun, S.; Daxin, E. The investigation of time-dependent springback for AC170PX aluminum alloy at room temperature. *Mater. Des.* **2016**, *93*, 118–127. [CrossRef]
11. Pinnola, F.P.; Vaccaro, M.S.; Barretta, R.; de Sciarra, F.M. Finite element method for stress-driven nonlocal beams. *Eng. Anal. Bound. Elem.* **2022**, *134*, 22–34. [CrossRef]
12. Liu, H.; Da-Xin, E. Modeling and Fenite-element Simulation of Time-dependent Springback of 1Cr18Ni9Ti Stainless Steel Tubes Based on Elasto-viscoplasticity. *J. Netshape Form. Eng.* **2015**, *6*, 65–69.
13. Kichenin, J.; Van Dang, K.; Boytard, K. Finite-element simulation of a new two-dissipative mechanisms model for bulk medium-density polyethylene. *J. Mater. Sci.* **1996**, *31*, 1653–1661. [CrossRef]
14. Fu, Z.; Da-xin, E. Time-dependent Springback Tests and the Finite Element Exploration of DP600 after Bending. *J. Netshape Form. Eng.* **2016**, *8*, 59–62.
15. Li, H.; Zhang, L.; Chen, G.; Ma, J.; Wei, D.; Bian, T.; Yang, J.; Wu, C.; Yang, H. Time-dependent springback of high strength titanium tubular materials: Experiment and modeling. *J. Mater. Processing Technol.* **2022**, *299*, 117354. [CrossRef]
16. Sun, S. A novel model based on viscoelastic theory to predict the time-dependent springback for dp600 steel sheet. *Acta Metall. Sin.* **2015**, *51*, 1356–1364. [CrossRef]

17. Shin, J.H.; Cho, Y.H. Machine-Learning-Based Coefficient of Performance Prediction Model for Heat Pump Systems. *Appl. Sci.* **2021**, *12*, 362. [CrossRef]
18. Li, B.; Gong, A.; Zeng, T.; Bao, W.; Xu, C.; Huang, Z. A Zoning Earthquake Casualty Prediction Model Based on Machine Learning. *Remote Sens.* **2021**, *14*, 30. [CrossRef]
19. Liu, Q.; Feng, X.; Chen, J. Interfacial Friction Prediction in a Vertical Annular Two-Phase Flow Based on Support Vector Regression Machine. *Water* **2021**, *13*, 3609. [CrossRef]
20. Liu, T.; Cai, Z.; Wang, N.; Jia, R.; Tian, W. Prediction Method of Coal Dust Explosion Flame Propagation Characteristics Based on Principal Component Analysis and BP Neural Network. *Math. Probl. Eng.* **2022**, *2022*, 1–8. [CrossRef]
21. Wang, Z.; Wang, F.; Su, S. Solar irradiance short-term prediction model based on BP neural network. *Energy Procedia* **2011**, *12*, 488–494. [CrossRef]
22. Liu, Y.; Xie, F.; Xie, C.; Peng, M.-J.; Wu, G.; Xia, H. Prediction of time series of NPP operating parameters using dynamic model based on BP neural network. *Ann. Nucl. Energy* **2015**, *85*, 566–575. [CrossRef]
23. Lu, X.H.; Wang, Y.Q.; Li, J.; Zhou, Y.; Ren, Z.J.; Liang, S.Y. Three-dimensional coordinate measurement algorithm by optimizing BP neural network based on GA. *Eng. Comput.* **2019**, *36*, 2066–2083. [CrossRef]
24. Han, Z.; Hong, L.; Meng, J.; Li, Y.; Gao, Q. Temperature drift modeling and compensation of capacitive accelerometer based on AGA-BP neural network. *Measurement* **2020**, *164*, 108019. [CrossRef]
25. Whitley, D. A genetic algorithm tutorial. *Stat. Comput.* **1994**, *4*, 65–85. [CrossRef]
26. Katoch, S.; Chauhan, S.S.; Kumar, V. A review on genetic algorithm: Past, present, and future. *Multimed. Tools Appl.* **2021**, *80*, 8091–8126. [CrossRef] [PubMed]
27. Fang, Y.C. Forecast of Foreclosure Property Market Trends during the Epidemic Based on GA-BP Neural Network. *Sci. Program.* **2022**, *2022*, 1–7. [CrossRef]
28. Wang, S.; Zhang, N.; Wu, L.; Wang, Y. Wind speed forecasting based on the hybrid ensemble empirical mode decomposition and GA-BP neural network method. *Renew. Energy* **2016**, *94*, 629–636. [CrossRef]
29. He, F.; Zhang, L. Mold breakout prediction in slab continuous casting based on combined method of GA-BP neural network and logic rules. *Int. J. Adv. Manuf. Technol.* **2018**, *95*, 4081–4089. [CrossRef]
30. Rizzo, F.J.; Shippy, D.J. An application of the correspondence principle of linear viscoelasticity theory. *SIAM J. Appl. Math.* **1971**, *21*, 321–330. [CrossRef]
31. Christensen, R. *Theory of Viscoelasticity: An Introduction*; Elsevier: Amsterdam, The Netherlands, 2012.
32. Song, Y. Load-deflection model for T-section rail press straightening process under lateral loads. *Clust. Comput.* **2019**, *22*, 2955–2961. [CrossRef]
33. Maleki, E.; Unal, O.; Kashyzadeh, K.R. Fatigue behavior prediction and analysis of shot peened mild carbon steels. *Int. J. Fatigue* **2018**, *116*, 48–67. [CrossRef]
34. Garson, G.D. Interpreting neural-network connection weights. *AI Expert* **1991**, *6*, 47–51.